

Cite this: *J. Mater. Chem. C*, 2022, **10**, 3560

## Facile ACQ-to-AIE transformation via diphenylphosphine (DPP) modification with versatile properties†

Fangjun Ye,<sup>a</sup> Chengzhen Shen,<sup>a</sup> Jianxin Guan,<sup>a</sup> Yiming Liu,<sup>a</sup> Xiaoge Wang,<sup>a</sup> Jingtian Wang,<sup>b</sup> Ming Cong,<sup>b</sup> Weibin Wang,<sup>b</sup> Ting Zhang,<sup>b</sup> Bo Zou,<sup>b</sup> Junrong Zheng<sup>b</sup> and Yuguo Ma<sup>b</sup>

Aggregation-induced emission (AIE) materials have attracted increasing research attention due to their broad application potential. The major design strategy for AIE luminogens (AIEgens) is incorporating molecular rotors, such as tetraphenylethylene (TPE) and triphenylamine (TPA), into conjugated skeletons to decrease intermolecular  $\pi$ - $\pi$  interactions. Therefore, the diversity of AIEgens is usually determined by the types of molecular rotors. Herein, we report a new molecular rotor, diphenylphosphine (DPP), that can be incorporated facilely into a typical aggregation-caused quenching (ACQ) luminophore to facilitate ACQ-to-AIE transformation. Due to the large steric hindrance and  $sp^3$  hybrid conformation of diphenylphosphine, the intermolecular  $\pi$ - $\pi$  interaction is limited to a certain extent; the photoluminescence quantum yields of our AIEgens range from 10.3% to 47.0%. Furthermore, the luminescent color of the molecules can be tuned from blue to orange by adjusting the electron-donating/withdrawing strength of the substituent groups. At the same time, the AIEgens also exhibit novel pressure-induced emission enhancement (PIEE) properties. The rapid intersystem crossing (ISC) process was explored as the DPP-based AIE mechanism by ultrafast IR spectroscopy. To our best knowledge, this is the first systematic study of a general strategy to realize ACQ-to-AIE transformation by using the DPP group, which greatly increases the diversity of AIEgens as well as their potential applications.

Received 3rd December 2021,  
Accepted 26th January 2022

DOI: 10.1039/d1tc05810j

rsc.li/materials-c

## Introduction

The majority of luminophores emits strongly in dilute solutions but weakly in aggregated states. This phenomenon, called the aggregation-caused quenching (ACQ) effect,<sup>1</sup> is usually caused by their strong intermolecular  $\pi$ - $\pi$  interactions and severely hampers the applications of ACQ molecules.<sup>2,3</sup> To solve this problem, a new class of luminophores was reported by Tang *et al* in 2001,<sup>4</sup> which showed negligible luminescence in solution but emitted intensely in the solid state. The phenomenon of aggregation-induced emission (AIE) was found very early<sup>5,6</sup> and has attracted more and more attention.<sup>7</sup> Solid-state luminescent materials consisting of AIEgens have developed rapidly by virtue of their promising prospects in the fields of

optoelectronic devices,<sup>8-12</sup> chemical sensing<sup>13-16</sup> and bio-imaging.<sup>17-20</sup> Structurally, AIEgens usually have a twisted molecular skeleton and a freely-rotating molecular rotor moiety. The former can inhibit intermolecular  $\pi$ - $\pi$  interactions, and the latter can promote non-radiative transition in solution, so as to achieve high contrast between non-luminescence in solution and strong solid luminescence. Besides tetraphenylethylene (TPE) and triphenylamine (TPA), a few other rotors have also been reported. The finite types of molecular rotors hinder the further development of new AIEgens.

ACQ luminophores (ACQphores) exhibit rich variety and excellent photophysical properties.<sup>2,3</sup> To circumvent the limitation of their application, the idea of converting them into AIE-active molecules is natural to occur.<sup>11,21-27</sup> There are some approaches reported so far to realize such a transformation by incorporating twisted molecule rotors,<sup>19,28,29</sup> bulky substituents<sup>30</sup> into planar ACQphores and some unique AIEgens with novel molecular design<sup>10,31-36</sup> to suppress the formation of  $\pi$ -aggregates by changing the molecular packing state.<sup>37</sup> In particular, constructing new AIEgens by combining typical molecule rotors, like TPE and TPA, with ACQphores<sup>38-43</sup> is effective. TPE-modified AIEgens can be usually used to explore multi-stimuli responsive luminescent

<sup>a</sup> College of Chemistry and Molecular Engineering, Beijing National Laboratory for Molecular Sciences, Peking University, Beijing 100871, China.  
E-mail: ygma@pku.edu.cn

<sup>b</sup> State Key Laboratory of Superhard Materials, College of Physics, Jilin University, Changchun 130012, China

† Electronic supplementary information (ESI) available. CCDC 2119796–2119799. For ESI and crystallographic data in CIF or other electronic format see DOI: 10.1039/d1tc05810j

materials due to their twisted molecular conformation and high fluorescence contrast between the solution and solid states.<sup>44</sup> However, these molecules have relatively poor wavelength adjustability due to their insignificant electronic effects. TPA-modified AIEgens can solve this problem well because of the strong electron-donating ability of the TPA group. But the  $sp^2$  hybridization configuration of nitrogen atoms may limit their intramolecular motions, leading to low luminescence contrast in the solid and liquid states. It is necessary to develop a new molecular rotor combining the advantages of the above two molecular rotors.

Herein, we report a novel approach for ACQ-to-AIE transformation by incorporating diphenylphosphine (DPP) into common ACQ fluorophores. Similar to the diphenylamine (DPA) or triphenylamine (TPA) system, DPP was taken as an electron-donor owing to the rich electron density of the phosphorus atom. What's more, the P atom has a larger volume and more atom orbitals than the N atom. DPP-containing molecules present a triangular pyramid configuration due to the  $sp^3$  hybridization of P atoms and show a greater freedom of motion, compared with DPA-containing molecules with a planar three-blade-propeller configuration (Fig. 1a). Accordingly, the P-containing system shows a more prominent AIE effect with a larger emission enhancement factor,  $\alpha_{AIE}$ , which is calculated from the emission intensity ratio between the solution state and aggregated state.<sup>42,45</sup> Coumarin was chosen as a model luminophore because of its typical ACQ properties with a simple structure and multiple modification positions.<sup>3</sup> New AIEgens were simply and efficiently obtained *via* a one-step optimized C–P coupling reaction (Fig. 1b). These molecules display strong emission intensity owing to the large steric hindrance of the DPP group to avoid  $\pi$ – $\pi$  interactions effectively in the solid state and undetectable luminescence in THF solution due to the low energy barrier of the intramolecular motion. The emission wavelength can be tuned by controlling the D–A strength with different substituent groups. Although a

few examples of solid-state luminescence by DPP modification have been mentioned in the literature,<sup>46–49</sup> a systematic study of a general strategy to realize ACQ-to-AIE transformation by DPP-modification still needs to be explored. Furthermore, the AIEgens show novel pressure-induced emission enhancement (PIEE) characteristics by using the diamond anvil cell (DAC) technique. The molecular motions are further inhibited by applying external pressure, contributing to the emission enhancement similar to what has been reported in the literature.<sup>50–60</sup> The rapid intersystem crossing is the internal mechanism of non-luminescence in the solution state, which is different from the previous report that planarization leads to fluorescence quenching.<sup>41</sup>

## Results and discussion

### Synthesis and comparison of AIE properties

Using C–P coupling reaction under optimized conditions, a series of coumarin-as-the-core AIEgens modified with the DPP group were synthesized efficiently, which display a transition from ACQ to AIE (Table S1, †). At the same time, a molecule with a diarylamine substituent (**4-N**) was synthesized as a reference. It is worth mentioning that the same effect can be achieved with triphenylphosphine (TPP) modification. However, from the perspective of synthesis, DPP modification is more economical and convenient (Fig. S1, ESI†).

The luminescence spectra of **4-P** and **4-N** in THF/water mixtures with different water fractions ( $f_w$ ) were recorded (Fig. 2). The emission of **4-P** is undetectable in THF but intense in water-dominated solution, indicative of its typical AIE characteristics. The  $\alpha_{AIE}$  value of **4-P** is 42.8. However, the emission intensity of **4-N** at  $f_w = 99$  vol% is lower than that in THF with an  $\alpha_{AIE}$  value of 0.4. As revealed by the <sup>1</sup>H NMR spectra in Fig. S2 (ESI†), **4-P** and **4-N** show different motion features in solutions. The aromatic hydrogen signals of **4-P** display a broad peak in

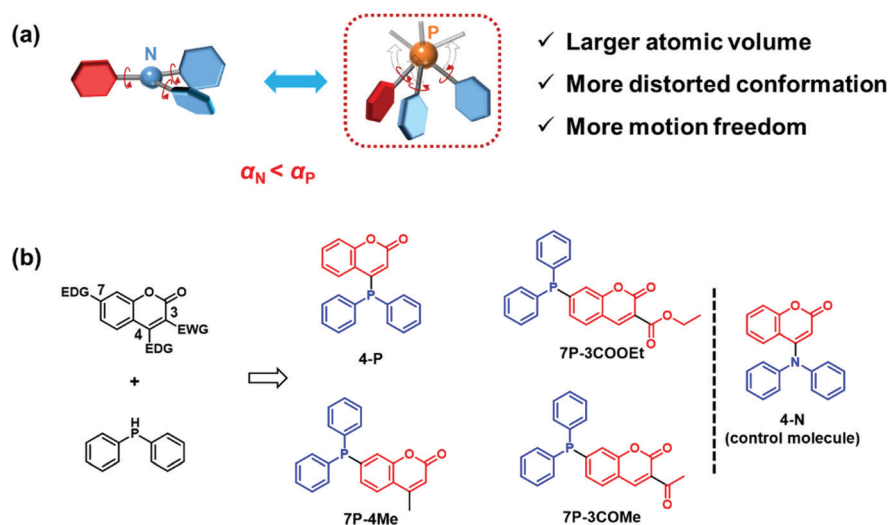


Fig. 1 (a) Different molecular configurations and motion modes between P- and N-containing luminophores. (b) Molecular structures of DPP-modified AIEgens.

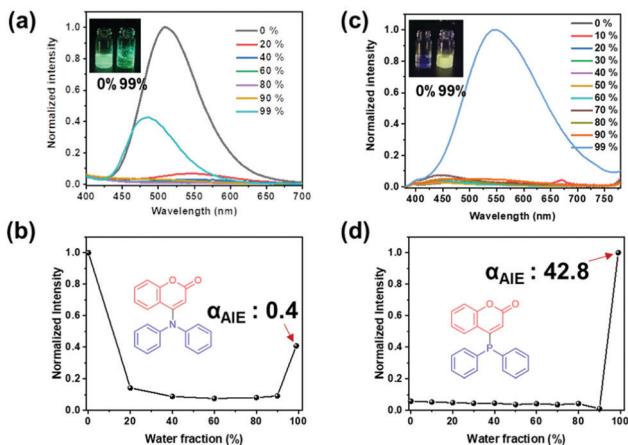


Fig. 2 (a) Luminescence spectra of **4-N** ( $10^{-5}$  M) in H<sub>2</sub>O/THF mixtures with different  $f_W$  values. (b) Luminescence intensity of **4-N** at 510 nm as a function of  $f_W$ . (c) Luminescence spectra of **4-P** ( $10^{-5}$  M) in H<sub>2</sub>O/THF mixtures with different  $f_W$  values. (d) Luminescence intensity of **4-P** at 550 nm as a function of  $f_W$ .

the region of  $\delta$  7.36–7.46 ppm, and the signal splitting becomes refined when decreasing the temperature, indicating the limitation of intramolecular motion. On the other hand, **4-N** shows more refined signal splitting, owing to the stronger electron delocalization effect and the restriction of intramolecular motions with a planar conformation. Faster motion and more motion modes will make it easier to cross energy barriers to reach fast energy dissipation pathways.<sup>61</sup> Consequently, compared with **4-N**, **4-P** shows a much higher contrast of emission intensity between different states. These results illustrate the reasonability of our molecule design for the new DPP-containing AIEgens. In the crystal structure of **4-P**, the aromatic nucleus distance between molecules is relatively short, and there is effective overlap area between the conjugated structures (Fig. S3, S20, ESI<sup>†</sup>). This means that modifying DPP at the 4-position of coumarin is difficult to completely inhibit the intermolecular  $\pi$ - $\pi$  interactions (3.44 Å). This is the reason that **4-P** has a relatively low photoluminescence quantum yield (PLQY 10.3%) in the solid state (Table S1, ESI<sup>†</sup>).

### AIE and mechanochromism

To improve the solid-state luminous efficiency, DPP was assembled at the 7-position of coumarin and the methyl group was introduced at the 4-position to obtain **7P-4Me**. The molecule **7P-4Me** was synthesized in only two steps with a satisfactory yield, giving an elevated PLQY (47.0%) in the crystalline state compared to **4-P**. As expected, **7P-4Me** demonstrates typical AIE features in THF/water mixture solutions (Fig. 3a and b). The single crystal X-ray diffraction (XRD) analysis shows that the **7P-4Me** crystal demonstrates a loose molecular stacking mode owing to the presence of DPP at the 7-position. There are two kinds of packing patterns ( $\alpha$ ,  $\beta$ ) in the adjacent layers and the distance between layers is up to 3.9 Å. From the top view, it can be seen that the conjugated structures do not have effective overlap area between layers, indicating the lack of

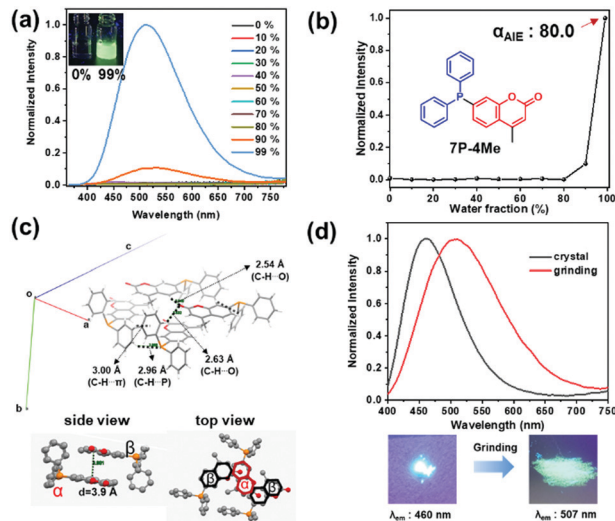


Fig. 3 (a) Luminescence spectra of **7P-4Me** ( $3.7 \times 10^{-5}$  M) in H<sub>2</sub>O/THF mixtures with different  $f_W$  values. (b) Luminescence intensity of **7P-4Me** at 510 nm as a function of  $f_W$ . (c) The crystal structure of **7P-4Me** including intermolecular interactions, layer distance and overlap area (hydrogen omitted for clarity). (d) The mechanochromic effect of **7P-4Me** upon grinding.

significant  $\pi$ - $\pi$  interactions. The crystal structure is stabilized by the strong C-H...O interaction (2.54 Å, 2.63 Å), C-H...P interaction (2.96 Å) and C-H... $\pi$  interaction (3.00 Å) (Fig. 3c and Fig. S4, S23, ESI<sup>†</sup>). The XRD results suggest that the PLQY of **7P-4Me** increases substantially due to the large steric hindrance of the DPP group at the 7-position of coumarin to avoid intermolecular  $\pi$ - $\pi$  interactions effectively. This suggests that the substituent site of DPP plays an important role in improving solid-state luminescence. Impressively, **7P-4Me** has an obvious mechanochromic effect. The emission peak of the crystalline state appears at 460 nm (blue), and is bathochromically shifted to 507 nm (green) after grinding (Fig. 3d). The powder X-ray diffraction (PXRD) experiments were performed to find the inherent mechanism. The diffraction signal of the **7P-4Me** crystal becomes weaker or even disappears after grinding (Fig. S5, ESI<sup>†</sup>). This suggests that the red-shift emission is caused by amorphization during the grinding process, and the molecular conformation becomes more planar, leading to the distinguished red-shift of the emission wavelength.

In addition, different electron-withdrawing groups were introduced at the 3-position of the coumarin core to tune the emission wavelength by regulating the D-A strength. **7P-3COMe** and **7P-3COOEt** were synthesized, and both of them show distinct AIE characteristics. The steric hindrance caused by the two electron withdrawing groups is different. Their emission wavelengths in the crystalline form are 554 nm and 603 nm respectively. The luminescence of **7P-3COMe** displays a bathochromic shift from 554 nm to 575 nm, whereas the luminescence of **7P-3COOEt** shows a hypsochromic shift from 603 nm to 597 nm upon grinding (Fig. S6 and S7, ESI<sup>†</sup>). The XRD analysis (Fig. S8, S9, S21 and S22, ESI<sup>†</sup>) indicates that **7P-3COOEt** has a looser packing mode than **7P-3COMe** due to

the steric hindrance of the ethoxy acyl group, which prevents  $\pi$ - $\pi$  interaction more effectively. This is probably the reason for **7P-3COOEt** having a higher PLQY. Remarkably, the emission wavelength can be tuned from blue to orange while retaining a relatively high PLQY in the solid state (Table S1, ESI<sup>†</sup>).

### PIEE phenomenon

Furthermore, all the above DPP-modified AIEgens show novel PIEE characteristics investigated with the DAC technique. Within the pressure threshold of 1.1 GPa for **7P-4Me**, 0.2 GPa for **7P-4Me**, 0.5 GPa for **7P-3COMe** and 0.6 GPa for **7P-3COOEt**, respectively, a conspicuous emission signal enhancement was detected (Fig. 4). All their UV-visible absorption spectra demonstrated distinct red shifts as the pressure increased. The tighter packing structure and pressure-induced conformational planarization are the main causes of the red-shift phenomena.<sup>62–65</sup> When the pressure was released to 0.0 GPa, the UV-vis spectra recovered to those at the initial 0.0 GPa, the same as the PL spectra (Fig. S10–S13, ESI<sup>†</sup>). The temperature dependent photoluminescence of **7P-4Me** in the solid state shows the same trend as that in a relatively low-pressure range (0–0.2 GPa), which supports the mechanism of pressure-induced restriction of intramolecular motion (Fig. S14, ESI<sup>†</sup>). Furthermore, from the *in situ* high-pressure IR spectroscopy, it can be inferred that the intermolecular hydrogen bond interaction increases due to the changes in the stretching vibration frequency of the carbonyl group  $\nu(\text{C}=\text{O})$  at  $1724\text{ cm}^{-1}$  (Fig. S15, ESI<sup>†</sup>). This may be the source of the limitation of intramolecular movement.

### AIE mechanism

Generally, the AIE phenomenon occurs as a consequence of multiple processes such as restriction of intramolecular motion (RIM),<sup>42,45,66</sup> twisted intramolecular charge transfer (TICT),<sup>16,39</sup> and conical intersection (CI).<sup>67,68</sup> The photophysical properties

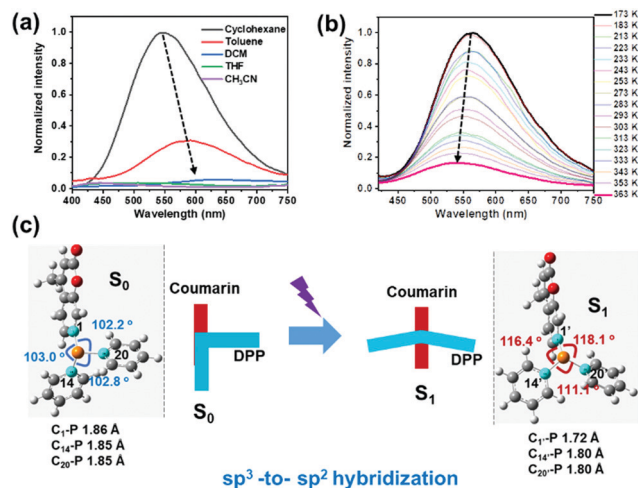


Fig. 5 (a) Emission spectra of **7P-4Me** ( $1.3 \times 10^{-5}$  M) with different solvents. (b) Temperature-dependent emission spectra of **7P-4Me** in degassed methylcyclohexane (the temperature range (173 K–363 K) is within the liquid phase range (147 K–374 K)). (c) Conformation optimization of the ground/excited state by the DFT calculation method: M06-2X/6-31g\*\*.

of **7P-4Me** were investigated in detail to gain deeper insight into the AIE mechanism (Fig. S16 and S17, ESI<sup>†</sup>). Its absorption peaks remain almost unchanged, while the emission spectra change significantly when altering the polarity of solvent. As the polarity of the solvent increases, the emission wavelength shows a red-shift tendency and the intensity decreases sharply. The emission signal displays a peak at 546 nm in cyclohexane, but in dichloromethane (DCM) nearly undetectable (Fig. 5a). This phenomenon is consistent with the TICT effect according to the literature.<sup>39,69</sup> With increasing solvent polarity, the molecular conformation of the excited state will be quickly distorted to an equilibrium state through a freely-rotating covalent bond, which is similar to the charge separation state, leading to the weakening or even quenching of the fluorescence intensity. The polarity of solvent is dependent on the temperature based on a previously reported study.<sup>70</sup> In the temperature-dependent emission spectra in methylcyclohexane (Fig. 5b), the emission wavelength exhibits a hypsochromic shift owing to the decrease of polarity. However, the emission intensity displays a decreasing tendency reverse to the TICT effect at elevated temperatures.<sup>70</sup> This means that the AIE phenomenon is not simply caused by TICT. Furthermore, to confirm the mechanism, calculations on the structures were carried out. M06-2X in combination with a 6-31g\*\* basis set (M06-2X/6-31g\*\*) was used to compute the ground and excited states of **7P-4Me**. The sum of the C1–P13–C14, C1–P13–C20 and C14–P13–C20 angles in the ground state is smaller than that in the excited state and the C1–P, C14–P and C20–P distances in the ground state are longer than those in the excited state (Fig. 5c). This means that the conformation has a sp<sup>3</sup>-to-sp<sup>2</sup> hybridization process under excitation with light and the molecule has a clear tendency to planarize.<sup>41</sup>

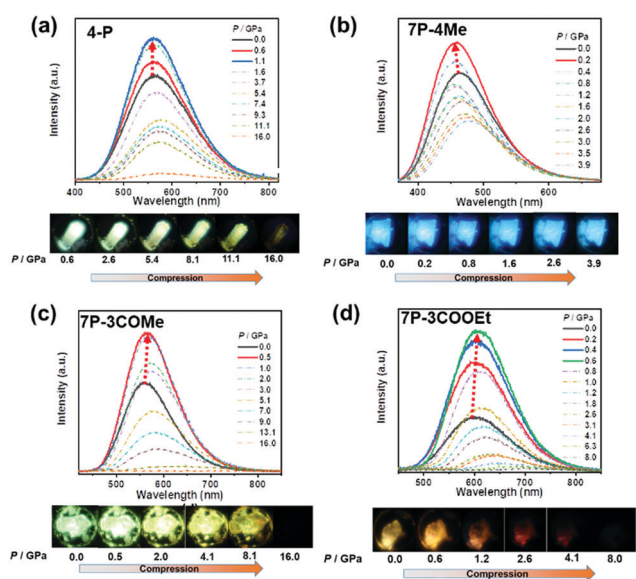


Fig. 4 Photophysical properties and PIEE characteristics of (a) **4-P**, (b) **7P-4Me**, (c) **7P-3COMe**, and (d) **7P-3COOEt**.

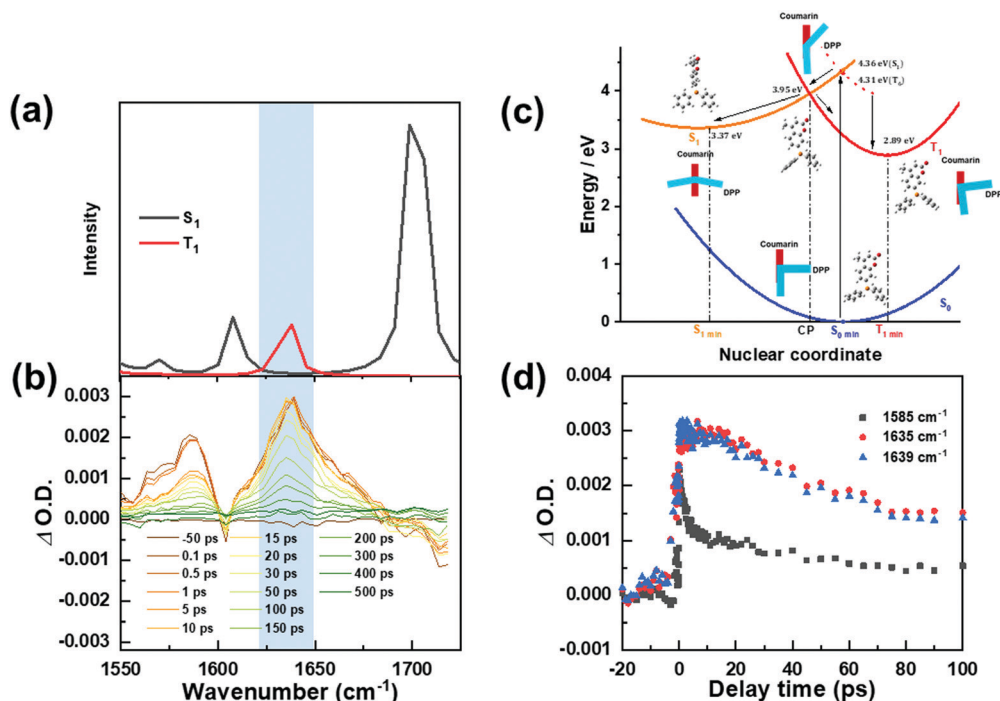


Fig. 6 (a) Vibration frequency analysis of the calculated **7P-4Me** in excited singlet and triplet states, method: M06-2X/6-31g\*\*, PCM in DCM. (b) Ultrafast IR spectra of **7P-4Me** in a dilute (59 mM) DCM solution after excitation with a wavelength of 360 nm. (c) Proposed photophysical process model in solution. (d) Signal decays of **7P-4Me** in DCM solution detected at different IR frequencies.

In order to explore the specific photophysical process more deeply, ultrafast IR spectroscopy was performed. The absorption peak at  $1735\text{ cm}^{-1}$  reaches a maximum at around 8 ps (Fig. 6b and d), which comes from a new species. Through theoretical calculation, it is believed to be most likely the excited triplet state (Fig. 6a). This assumption is further confirmed by low-temperature phosphorescence experiments (Fig. S18, ESI†). At 77 K, the DCM solution of **7P-4Me** produces bright phosphorescent emission, and the lifetime can reach 118 ms, which shows that **7P-4Me** can indeed undergo an effective ISC process and produce high concentrations of triplet excitons. Considering the huge changes in molecular conformation after light excitation, the spin-orbit coupling (SOC) constants between  $S_1$  and  $T_n$  based on the corresponding molecular geometries of  $S_{0\text{min}}$  and  $S_{1\text{min}}$  were calculated (Fig. S19, ESI†). The former geometry has a higher energy and SOC constant. This result indicates that the intersystem crossing (ISC) process is very fast as the conformational relaxation process, and increasing the temperature facilitates the process, leading to fluorescence weakening or even quenching (Fig. 5b). Thus, the theoretical model is proposed by calculation (Fig. 6c). The energy and the conformation between  $S_1$  and CP (crossing point between S and T) of **7P-4Me** are similar, which means that the free vibration and rotation of molecules in the solution may twist the DPP and finally increase the rate of ISC. While it's hard to occur in the solid state due to the close distance between molecules, it is easier to produce triplet states in solution and quench the luminescence. And in the solid state, the process may be inhibited owing to the intermolecular

interactions, resulting in bright fluorescence. These two factors finally make facile ACQ-to-AIE transformation possible for this series of compounds. The ISC process in the AIE system has been predicted in the literature.<sup>67</sup> It is speculated that the ISC process can be greatly accelerated by virtue of charge transfer properties and the heavy atom effect of P, and the fast ISC process maybe happens in other AIE systems.

## Conclusions

To conclude, ACQ-to-AIE transformation of the luminophore coumarin was realized simply *via* DPP-modification. A series of DPP-containing AIEgens, **4-P**, **7P-4Me**, **7P-3COME** and **7P-3COOEt**, were synthesized facily through optimized C-P coupling reaction, and their emission wavelengths can be tuned by adjusting the electron-donating/withdrawing strength of the substituent groups at the 3- or 7-positions. In addition, by virtue of the  $sp^3$  hybridization conformation of the P-containing molecules, these molecules all present a triangular pyramid configuration. They also exhibit mechanochromism and novel PIEE characteristics. The AIE mechanism was investigated by combination of experimental and theoretical methods. The rapid ISC process was proposed to play an important role of non-luminescence in the solution state based on the results of ultrafast IR spectroscopy. We believe that these DPP-containing AIEgens will exhibit a brilliant performance in diverse applications owing to their facile preparation, good

stability, distinguished AIE characteristics and excellent photophysical properties in the solid state.

## Author contributions

Y. Ma and F. Ye conceived the idea and designed experiments. Y. Ma, J. Zheng and B. Zou supervised the project. F. Ye prepared materials and performed the photophysical experiments. J. Zheng, C. Shen, F. Ye and Y. Liu performed the theoretical calculations. J. Guan performed the ultrafast experiments. X. Wang performed the XRD experiments. B. Zou, J. Wang, M. Cong, W. Wang and T. Zhang conducted the *in situ* high pressure experiments. F. Ye, Y. Liu and C. Shen analyzed data.

## Conflicts of interest

There are no conflicts to declare.

## Acknowledgements

This research was financially supported by the National Science Foundation of China (NSFC, 21871016, 21725304, 21627805, and 21821004) and MOST (2017YFA0204702). We also acknowledge the support from the High-performance Computing Platform of Peking University for the computational resources and the Analytical Instrumentation Center of Peking University for the characterization.

## Notes and references

- 1 T. Förster and K. Kasper, *Z. Phys. Chem.*, 1954, **1**, 275–277.
- 2 J. Chan, S. C. Dodani and C. J. Chang, *Nat. Chem.*, 2012, **4**, 973–984.
- 3 R. M. Christie and C.-H. Lui, *Dyes Pigm.*, 2000, **47**, 79–89.
- 4 J. D. Luo, Z. L. Xie, J. W. Y. Lam, L. Cheng, H. Y. Chen, C. F. Qiu, H. S. Kwok, X. W. Zhan, Y. Q. Liu, D. B. Zhu and B. Z. Tang, *Chem. Commun.*, 2001, 1740–1741.
- 5 G. C. Schmidt, *Ann. Phys.*, 1896, **294**, 103–130.
- 6 J. Stark and P. Lipp, *Z. Phys. Chem.*, 1913, **86**, 36–41.
- 7 J. Yang, M. Fang and Z. Li, *Aggregate*, 2020, **1**, 6–18.
- 8 Z. Zhao, S. Chen, X. Shen, F. Mahtab, Y. Yu, P. Lu, J. W. Y. Lam, H. S. Kwok and B. Z. Tang, *Chem. Commun.*, 2010, **46**, 686–688.
- 9 B. R. He, Z. F. Chang, Y. B. Jiang, X. F. Xu, P. Lu, H. S. Kwok, J. Zhou, H. Y. Qiu, Z. J. Zhao and B. Z. Tang, *Dyes Pigm.*, 2014, **106**, 87–93.
- 10 F. Song, Z. Xu, Q. Zhang, Z. Zhao, H. Zhang, W. Zhao, Z. Qiu, C. Qi, H. Zhang, H. H. Y. Sung, I. D. Williams, J. W. Y. Lam, Z. Zhao, A. Qin, D. Ma and B. Z. Tang, *Adv. Funct. Mater.*, 2018, **28**, 1800051.
- 11 W. Qin, J. W. Y. Lam, Z. Yang, S. Chen, G. Liang, W. Zhao, H. S. Kwok and B. Z. Tang, *Chem. Commun.*, 2015, **51**, 7321–7324.
- 12 Y. Liu, C. Mu, K. Jiang, J. Zhao, Y. Li, L. Zhang, Z. Li, J. Y. L. Lai, H. Hu, T. Ma, R. Hu, D. Yu, X. Huang, B. Z. Tang and H. Yan, *Adv. Mater.*, 2015, **27**, 1015–1020.
- 13 F. Sun, G. Zhang, D. Zhang, L. Xue and H. Jiang, *Org. Lett.*, 2011, **13**, 6378–6381.
- 14 H. Shi, J. Liu, J. Geng, B. Z. Tang and B. Liu, *J. Am. Chem. Soc.*, 2012, **134**, 9569–9572.
- 15 N. Zhao, J. W. Y. Lam, H. H. Y. Sung, H. M. Su, I. D. Williams, K. S. Wong and B. Z. Tang, *Chem. – Eur. J.*, 2014, **20**, 133–138.
- 16 K. Xue, C. Wang, J. Wang, S. Lv, B. Hao, C. Zhu and B. Z. Tang, *J. Am. Chem. Soc.*, 2021, **143**, 14147–14157.
- 17 H. Shi, R. T. Kwok, J. Liu, B. Xing, B. Z. Tang and B. Liu, *J. Am. Chem. Soc.*, 2012, **134**, 17972–17981.
- 18 S. Zhen, S. Wang, S. Li, W. Luo, M. Gao, L. G. Ng, C. C. Goh, A. Qin, Z. Zhao, B. Liu and B. Z. Tang, *Adv. Funct. Mater.*, 2018, **28**, 1706945.
- 19 Y. Li, S. Liu, H. Ni, H. Zhang, H. Zhang, C. Chuah, C. Ma, K. S. Wong, J. W. Y. Lam, R. T. K. Kwok, J. Qian, X. Lu and B. Z. Tang, *Angew. Chem., Int. Ed.*, 2020, **59**, 12822–12826.
- 20 H. Shi, N. Zhao, D. Ding, J. Liang, B. Z. Tang and B. Liu, *Org. Biomol. Chem.*, 2013, **11**, 7289–7296.
- 21 W. Qin, Z. Yang, Y. Jiang, J. W. Y. Lam, G. Liang, H. S. Kwok and B. Z. Tang, *Chem. Mater.*, 2015, **27**, 3892–3901.
- 22 S. Wang, X. Yan, Z. Cheng, H. Zhang, Y. Liu and Y. Wang, *Angew. Chem., Int. Ed.*, 2015, **54**, 13068–13072.
- 23 W. Qin, K. Li, G. Feng, M. Li, Z. Yang, B. Liu and B. Z. Tang, *Adv. Funct. Mater.*, 2014, **24**, 635–643.
- 24 G. Lin, P. N. Manghnani, D. Mao, C. Teh, Y. Li, Z. Zhao, B. Liu and B. Z. Tang, *Adv. Funct. Mater.*, 2017, **27**, 1701418.
- 25 X. Shi, S. H. P. Sung, M. M. S. Lee, R. T. K. Kwok, H. H. Y. Sung, H. Liu, J. W. Y. Lam, I. D. Williams, B. Liu and B. Z. Tang, *J. Mater. Chem. B*, 2020, **8**, 1516–1523.
- 26 S. Liu, G. Feng, B. Z. Tang and B. Liu, *Chem. Sci.*, 2021, **12**, 6488–6506.
- 27 Y. Shi, P. Sang, G. Yin, R. Gao, X. Liang, R. Brzozowski, T. Odom, P. Eswara, Y. Zheng, X. Li and J. Cai, *Adv. Opt. Mater.*, 2020, **8**, 2000855.
- 28 Z. Zhao, P. Lu, J. W. Y. Lam, Z. Wang, C. Y. K. Chan, H. H. Y. Sung, I. D. Williams, Y. Ma and B. Z. Tang, *Chem. Sci.*, 2011, **2**, 672–675.
- 29 C. Gao, G. Gao, J. Lan and J. You, *Chem. Commun.*, 2014, **50**, 5623–5625.
- 30 L. Zong, Y. Xie, C. Wang, J.-R. Li, Q. Li and Z. Li, *Chem. Commun.*, 2016, **52**, 11496–11499.
- 31 S. Zheng, T. Zhu, Y. Wang, T. Yang and W. Z. Yuan, *Angew. Chem., Int. Ed.*, 2020, **59**, 10018–10022.
- 32 J. Guo, J. Fan, X. Liu, Z. Zhao and B. Z. Tang, *Angew. Chem., Int. Ed.*, 2020, **59**, 8828–8832.
- 33 F. Ni, Z. Zhu, X. Tong, W. Zeng, K. An, D. Wei, S. Gong, Q. Zhao, X. Zhou and C. Yang, *Adv. Sci.*, 2019, **6**, 1801729.
- 34 M.-S. Yuan, D.-E. Wang, P. Xue, W. Wang, J.-C. Wang, Q. Tu, Z. Liu, Y. Liu, Y. Zhang and J. Wang, *Chem. Mater.*, 2014, **26**, 2467–2477.
- 35 S. Chen, N. Chen, Y. L. Yan, T. Liu, Y. Yu, Y. Li, H. Liu, Y. S. Zhao and Y. Li, *Chem. Commun.*, 2012, **48**, 9011–9013.

- 36 N. Xie, Y. Liu, R. Hu, N. L. C. Leung, M. Arseneault and B. Z. Tang, *Isr. J. Chem.*, 2014, **54**, 958–966.
- 37 Q. Li and Z. Li, *Acc. Chem. Res.*, 2020, **53**, 962–973.
- 38 S. Liu, Y. Li, R. T. K. Kwok, J. W. Y. Lam and B. Z. Tang, *Chem. Sci.*, 2021, **12**, 3427–3436.
- 39 R. Hu, E. Lager, A. Aguilar-Aguilar, J. Liu, J. W. Y. Lam, H. H. Y. Sung, I. D. Williams, Y. Zhong, K. S. Wong, E. Peña-Cabrera and B. Z. Tang, *J. Phys. Chem. C*, 2009, **113**, 15845–15853.
- 40 D. Ding, K. Li, B. Liu and B. Z. Tang, *Acc. Chem. Res.*, 2013, **46**, 2441–2453.
- 41 T. Machida, T. Iwasa, T. Taketsugu, K. Sada and K. Kokado, *Chem. – Eur. J.*, 2020, **26**, 8028–8034.
- 42 J. Mei, N. L. C. Leung, R. T. K. Kwok, J. W. Y. Lam and B. Z. Tang, *Chem. Rev.*, 2015, **115**, 11718–11940.
- 43 S. Liu, C. Chen, Y. Li, H. Zhang, J. Liu, R. Wang, S. T. H. Wong, J. W. Y. Lam, D. Ding and B. Z. Tang, *Adv. Funct. Mater.*, 2019, **30**, 1908125.
- 44 G. Huang, Y. Jiang, S. Yang, B. S. Li and B. Z. Tang, *Adv. Funct. Mater.*, 2019, **29**, 1900516.
- 45 Y.-Y. Liu, X. Zhang, K. Li, Q. Peng, Y. Qin, H. Hou, S.-Q. Zang and B. Z. Tang, *Angew. Chem., Int. Ed.*, 2021, **60**, 2–9.
- 46 P. Natarajan, *Anal. Methods*, 2014, **6**, 2432–2435.
- 47 P. Xue, P. Wang, P. Chen, J. Ding and R. Lu, *RSC Adv.*, 2016, **6**, 51683–51686.
- 48 T. Schillmöller, P. N. Ruth, R. Herbst-Irmer and D. Stalke, *Chem. – Eur. J.*, 2020, **26**, 17390–17398.
- 49 C. Xing, J. Liu, F. Chen, Y. Li, C. Lv, Q. Peng, H. Hou and K. Li, *Chem. Commun.*, 2020, **56**, 4220–4223.
- 50 X. Fan, J. Sun, F. Wang, Z. Chu, P. Wang, Y. Dong, R. Hu, B. Z. Tang and D. Zou, *Chem. Commun.*, 2008, 2989–2991.
- 51 Q. Wang, S. Li, L. He, Y. Qian, X. Li, W. Sun, M. Liu, J. Li, Y. Li and G. Yang, *ChemPhysChem*, 2008, **9**, 1146–1152.
- 52 H. Yuan, K. Wang, K. Yang, B. Liu and B. Zou, *J. Phys. Chem. Lett.*, 2014, **5**, 2968–2973.
- 53 Y. Gu, K. Wang, Y. Dai, G. Xiao, Y. Ma, Y. Qiao and B. Zou, *J. Phys. Chem. Lett.*, 2017, **8**, 4191–4196.
- 54 S. Zhang, Y. Dai, S. Luo, Y. Gao, N. Gao, K. Wang, B. Zou, B. Yang and Y. Ma, *Adv. Funct. Mater.*, 2017, **27**, 1602276.
- 55 Z. Ma, Z. Liu, S. Lu, L. Wang, X. Feng, D. Yang, K. Wang, G. Xiao, L. Zhang, S. A. T. Redfern and B. Zou, *Nat. Commun.*, 2018, **9**, 4506.
- 56 Y. Shi, Z. Ma, D. Zhao, Y. Chen, Y. Cao, K. Wang, G. Xiao and B. Zou, *J. Am. Chem. Soc.*, 2019, **141**, 6504–6508.
- 57 Y. Fang, L. Zhang, L. Wu, J. Yan, Y. Lin, K. Wang, W. L. Mao and B. Zou, *Angew. Chem., Int. Ed.*, 2019, **58**, 15249–15253.
- 58 L. Zhang, C. Liu, L. Wang, C. Liu, K. Wang and B. Zou, *Angew. Chem., Int. Ed.*, 2018, **57**, 11213–11217.
- 59 N. Li, Y. Gu, Y. Chen, L. Zhang, Q. Zeng, T. Geng, L. Wu, L. Jiang, G. Xiao, K. Wang and B. Zou, *J. Phys. Chem. C*, 2019, **123**, 6763–6767.
- 60 H. Yang, Z. Sun, C. Lv, M. Qile, K. Wang, H. Gao, B. Zou, Q. Song and Y. Zhang, *ChemPlusChem*, 2018, **83**, 132–139.
- 61 J. Guan, C. Shen, J. Peng and J. Zheng, *J. Phys. Chem. Lett.*, 2021, **12**, 4218–4226.
- 62 Y. Liu, Q. Zeng, B. Zou, Y. Liu, B. Xu and W. Tian, *Angew. Chem., Int. Ed.*, 2018, **57**, 15670–15674.
- 63 Y. Sagara and T. Kato, *Nat. Chem.*, 2009, **1**, 605–610.
- 64 J. P. Schmidtke, J.-S. Kim, J. Gierschner, C. Silva and R. H. Friend, *Phys. Rev. Lett.*, 2007, **99**, 167401.
- 65 Y. Q. Dong, J. W. Y. Lam and B. Z. Tang, *J. Phys. Chem. Lett.*, 2015, **6**, 3429–3436.
- 66 J. Mei, Y. Hong, J. W. Lam, A. Qin, Y. Tang and B. Z. Tang, *Adv. Mater.*, 2014, **26**, 5429–5479.
- 67 S. Suzuki, S. Sasaki, A. S. Sairi, R. Iwai, B. Z. Tang and G. I. Konishi, *Angew. Chem., Int. Ed.*, 2020, **59**, 9856–9867.
- 68 J. Guan, R. Wei, A. Prlj, J. Peng, K.-H. Lin, J. Liu, H. Han, C. Corminboeuf, D. Zhao, Z. Yu and J. Zheng, *Angew. Chem., Int. Ed.*, 2020, **59**, 14903–14909.
- 69 Y. Qian, M. M. Cai, L. H. Xie, G. Q. Yang, S. K. Wu and W. Huang, *ChemPhysChem*, 2011, **12**, 397–404.
- 70 A. Kowski, B. Kukliński and P. Bojarski, *Chem. Phys. Lett.*, 2008, **455**, 52–54.
- 71 Y. Zhao and D. G. Truhlar, *Theor. Chem. Acc.*, 2008, **120**, 215–241.